HHS Public Access

Author manuscript

Nat Commun. Author manuscript; available in PMC 2013 July 29.

Published in final edited form as:

Nat Commun. 2013 ; 4: 1403. doi:10.1038/ncomms2413.

Src activation by β-adrenoreceptors is a key switch for tumor metastasis

Guillermo N. Armaiz-Pena[1], **Julie K. Allen**[1,10], **Anthony Cruz**[7], **Rebecca L. Stone**[1], **Alpa M. Nick**[1], **Yvonne G. Lin**[1], **Liz Y. Han**[1], **Lingegowda S. Mangala**[1,6], **Gabriel J. Villares**[2,10], **Pablo Vivas-Mejia**[3,16], **Cristian Rodriguez-Aquayo**[3], **Archana S. Nagaraja**[1,10], **Kshipra M. Gharpure**[1,10], **Zheng Wu**[11,12], **Robert D. English**[11], **Kizhake V. Soman**[11,12], **Mian M. K. Shazhad**[1], **Maya Zigler**[2,10], **Michael T. Deavers**[4], **Alexander Zien**[9], **Theodoros G. Soldatos**[9], **David B. Jackson**[9], **John E. Wiktorowicz**[11,12], **Madeline Torres-Lugo**[8], **Tom Young**[17], **Koen De Geest**[13], **Gary E. Gallick**[5], **Menashe Bar-Eli**[2], **Gabriel Lopez-Berestein**[2,3,6], **Steve W. Cole**[14], **Gustavo E. Lopez**[7], **Susan K. Lutgendorf**[13,15], and **Anil K. Sood**[1,2,6,*]

[1]Department of Gynecologic Oncology & Reproductive Medicine, The University of Texas M. D. Anderson Cancer Center, Houston, Texas 77030, USA

[2]Department of Cancer Biology, The University of Texas M. D. Anderson Cancer Center, Houston, Texas 77030, USA

[3]Department of Experimental Therapeutics, The University of Texas M. D. Anderson Cancer Center, Houston, Texas 77030, USA

[4]Department of Pathology, The University of Texas M. D. Anderson Cancer Center, Houston, Texas 77030, USA

[5]Department of Genitourinary Medical Oncology, The University of Texas M. D. Anderson Cancer Center, Houston, Texas 77030, USA

[6]Center for RNA Interference and Non-coding RNA, The University of Texas M. D. Anderson Cancer Center, Houston, Texas 77030, USA

[7]Department of Chemistry, University of Puerto Rico, Mayaguez, Puerto Rico 00681, USA

[8]Department of Chemical Engineering, University of Puerto Rico, Mayaguez, Puerto Rico 00681, USA

[9]Molecular Health GmbH, Belfortstr. 2, 69115 Heidelberg, Germany

[*]Correspondence and requests for materials should be addressed to A.K.S. (asood@mdanderson.org).

Author Contributions

G.N.A-P. designed the studies, performed experiments and wrote the manuscript. A.C., M.T-L., T.Y. and G.E.L. designed and performed structural modeling analyses and edited the manuscript. Z.W, R.D.E., K.V.S. and J.E.W. performed 2D gel analyses and mass spectrometry studies and edited the manuscript. D.B.J., T.G.S. and A.Z. analyzed the proteomics data and performed the adverse event dataset bioinformatics analysis. Y.G.L., L.Y.H., A.M.N., R.L.S., L.S.M., J.K.A., A.S.N., K.M.G and M.M.K.S. performed experiments and edited the manuscript. P.V-M, C.R.-A. and G.L-B. performed siRNA incorporations and edited the manuscript. G.J.V., M.Z. and M.B-E. designed and performed plasmid transfections and edited the manuscript. M.T.D. performed the immunohistochemical analysis and edited the manuscript. K.D.G., G.E.G, S.W.C., S.K.L. and A.K.S. designed the overall study, analyzed data and edited the manuscript.

The authors declare no competing financial interests.

[10]Cancer Biology Program, Graduate School of Biomedical Sciences, The University of Texas Health Science Center, Houston, Texas 77030, USA

[11]Biomolecular Resource Facility, The University of Texas Medical Branch, Galveston, Texas 77555, USA

[12]Department of Biochemistry and Molecular Biology, The University of Texas Medical Branch, Galveston, Texas 77555, USA

[13]Division of Gynecologic Oncology, Department of Obstetrics and Gynecology, University of Iowa, Iowa City, Iowa 52242, USA

[14]Department of Medical Oncology Hematology, University of California, Los Angeles, California 90095, USA

[15]Department of Psychology, Urology, and Holden Comprehensive Cancer Center, University of Iowa, Iowa City, Iowa 52242, USA

[16]Department of Biochemistry and Cancer Center, Medical Sciences Campus, University of Puerto Rico, San Juan, Puerto Rico 00935, USA

[17]Department of Chemistry, Lehman College, Bronx, New York 10468, USA

Abstract

Norepinephrine (NE) can modulate multiple cellular functions important for cancer progression; however, how this single extracellular signal regulates such a broad array of cellular processes is unknown. Here, we identify Src as a key regulator of phosphoproteomic signaling networks activated in response to beta-adrenergic signaling in cancer cells. These results also identify a new mechanism of Src phosphorylation that mediates beta-adrenergic/PKA regulation of downstream networks, thereby enhancing tumor cell migration, invasion and growth. In human ovarian cancer samples, high tumoral NE levels were correlated with high $pSrc^{Y419}$ levels. Moreover, among cancer patients, the use of beta blockers was significantly associated with reduced cancer-related mortality. Collectively, these data provide a pivotal molecular target for disrupting neural signaling in the tumor microenvironment.

INTRODUCTION

The tumor microenvironment is an important determinant of cancer progression, and microenvironmental distribution of neural and endocrine signals has now been identified as a key mediator of these dynamics[1,2]. For example, signaling resulting from activation of beta-adrenergic receptors (ADRB) by norepinephrine affects a broad array of processes involved in the progression of various cancer types[1,2]. However, the diversity of intracellular signaling pathways and cellular processes modulated by this single extracellular signal is surprising. For example, our previous work determined that sympathetic nervous system activity can directly enhance the pathogenesis of ovarian carcinoma by protecting tumor cells from anoikis [3] promoting tumor cell invasion[4–6] and tumor-associated angiogenesis[2,7]. We found that these effects were mediated through activation of tumor cell ADRB2, but its downstream signaling pathways are not well understood.

Here, we sought to determine key regulators of the cellular phosphoproteome following norepinephrine-stimulation of ADRB in cancer cells. We demonstrate that ADRB signaling leads to Src activation by a unique PKA-mediated mechanism, which is critical to the regulation of phosphoproteomic networks associated with ovarian cancer progression.

RESULTS

Norepinephrine activated signaling networks

Following treatment of SKOV3ip1 cells with norepinephrine (NE), proteins from treated and untreated cells were separated by 2D gel electrophoresis and stained for total and phosphorylated proteins (Supplementary Fig. S1a–b). Quantitative analyses of these samples, followed by mass spectrometry analysis identified 24 proteins with altered expression levels and 39 with differential phosphorylation (Supplementary Tables S1–2 and Supplementary Data 1–2). For each of these proteins, we identified kinases that may be upstream by up to two levels (the kinase targets another kinase which targets the protein). To identify putative key mediators, all involved kinases were scored by the number of identified downstream proteins. The highest score was achieved for Src (Fig. 1 and Supplementary Fig. S2a). To validate this finding, lysates from NE-treated tumor cells were subjected to immunoblotting, which confirmed the results obtained in our analysis (Supplementary Fig. S2b). Additionally, treatment with either dasatinib or Src siRNA abrogated NE-induced changes (Supplementary Fig. S2b). Next, we sought to determine the functional and biological roles of Src in promoting tumor growth in response to increased adrenergic signaling.

Beta adrenergic receptors mediate NE-induced Src activation

We first examined Y419 phosphorylation following NE stimulation. Since ovarian cancer cells do not produce NE (data not shown), we exposed cells to various NE concentrations known to be present in ovarian tissues and tumors under physiological and stress conditions[2,8]. In the ADRB-positive HeyA8 and SKOV3ip1 human ovarian cancer cells [2,9], $pSrc^{Y419}$ levels increased markedly (at least 3-fold) following exposure to 100 nM - 10 μM NE (Fig. 2a and Supplementary Fig. S3a). These increases are comparable to those seen by growth factor-mediated Src phosphorylation, as observed in Supplementary Fig. S3b. To show that Y419 phosphorylation leads to Src activation, we performed a kinase assay where focal adhesion kinase (FAK) was exposed to Src or a combination of Src with AP23846. Upon interaction with Src, FAK^{Y397} phosphorylation was substantially increased, while AP23846 blocked this effect (Supplementary Fig. S3c). Additionally, we show that FAK exposure to Src results in increased phosphorylation at Y925 that is not seen in the absence of ATP (Supplementary Fig. S3c). Similar responses to NE with regard to Y419 phosphorylation were noted with ADRB-positive breast cancer and melanoma cell lines (Supplementary Fig. S3d). In contrast, NE stimulation of the ADRB-deficient A2780-PAR cells[2] or hydrocortisone treatment of SKOV3ip1 cells did not increase $pSrc^{Y419}$ levels (Supplementary Fig. S3e and data not shown). Propranolol blocked NE-mediated Src activation (Supplementary Fig. S3e). Given the known role of $pSrc^{Y530}$ dephosphorylation in Src activation, we also probed for $pSrc^{Y530}$ following NE stimulation. There was no change in $pSrc^{Y530}$ phosphorylation, suggesting that the NE-induced Src activation was

solely mediated by phosphorylation at Y419 (Supplementary Fig. S3f,g). To further corroborate these findings, HeyA8 cells were treated with isoproterenol (10 μM), which resulted in Src^{Y419} phosphorylation within 5 min (Supplementary Fig. S3h). Butoxamine, blocked the NE-induced Src activation (Fig. 2b). To examine the specificity of ADRB receptors in mediating NE-induced activation of Src, we utilized ADRB1- or ADRB2-targeted small interfering RNA (siRNA) capable of reducing levels of each protein by >80% (Supplementary Fig S3i). Similar to the effects with inhibitors, ADRB1 and ADRB2 siRNA abrogated NE-induced Src activation (Fig. 2c). Next, we created stable clones of A2780-PAR cells transfected with an ADRB2 construct. After confirming ADRB2 expression (Supplementary Fig. S3j), we treated these cells with NE, which resulted in increased Src^{Y419} phosphorylation (Supplementary Fig. S3k).

NE-induced Src activation is mediated by cAMP/PKA

We next performed a series of experiments to delineate the signaling pathway involved in NE-mediated Src activation. Treatment of SKOV3ip1 cells with forskolin resulted in rapid Src^{Y419} phosphorylation (Supplementary Fig. S3l). To test whether PKA was involved in NE-mediated Src activation, cells were treated with dibutyryl-cAMP (dbcAMP), resulting in rapid Src^{Y419} phosphorylation (Fig. 2d). Furthermore, PKA silencing by siRNA or PKA inhibitors prevented NE-mediated Src activation (Fig. 2e and Supplementary Fig. S3m–n). Immunofluorescence analyses verified that upon NE stimulation, Src localizes to the focal adhesions in SKOV3ip1 cells (Fig. 2f–g and Supplementary Fig. S3o).

$pSrc^{S17}$ is required for NE-induced Src activation

Since PKA is a serine-threonine kinase, the paradoxical increase in Src tyrosine phosphorylation prompted us to consider potential underlying mechanisms. Src contains a single consensus PKA site at residues surrounding S17 (Supplementary Fig. S4a)[10]. To test whether NE and dbcAMP mediated induction of Src^{S17} phosphorylation was PKA-dependent, we treated HeyA8 cells with NE or dbcAMP. Both treatments rapidly increased $pSrc^{S17}$ levels (Fig. 3a and Supplementary Fig. S4b). Furthermore, in ADRB2-null A2780-PAR cells stably transfected with ADRB2, NE stimulation rapidly increased PKA activity, Src^{S17} phosphorylation, and Src activation (Supplementary Fig. S4c–d). To determine whether Ser17 phosphorylation is a prerequisite for NE-induced Src^{Y419} phosphorylation, mouse embryonic fibroblast cells null for Src, Yes, or Fyn (SYF) were transfected with plasmids containing either wild-type (WT) Src or Src mutated at S17 (S17A). To verify that NE could increase PKA activity in SYF cells, we measured phospho-PKA substrate levels in these cells. As expected, NE rapidly increased the levels of phospho-PKA substrates (Supplementary Fig. S3e). In addition, after verifying the transfection efficiency and confirming that WT and S17A Src were transiently expressed at similar levels (Supplementary Fig. S4f–g), we exposed them to NE or dbcAMP. Src^{Y419} and Src^{S17} were rapidly phosphorylated in WT Src-expressing cells following NE treatment, but not in the S17A Src-transfected cells (Fig. 3b,c and Supplementary Fig. S4h).

Interaction between pS17 and Src exposes Y419

The contribution of the Src N-terminus, where S17 resides, and specifically its unique domain to Src activation is not known, as the reported Src crystal structure does not include

the first 82 amino acid residues[11]. To understand how S17 phosphorylation might lead to subsequent Y419 phosphorylation, we performed molecular dynamic simulations. First, we obtained the atomic coordinates of c-Src from the Protein Data Bank (Code:2SRC)[12], and proceeded to eliminate phospho-aminophosphonic acid-adenylate ester (ANP) and water molecules, leaving Src in its inactive form (Figure 4a). Subsequently, we ran preliminary simulations with a computer designed full-length N-terminal attached to the known Src crystal structure. After performing extensive annealing molecular dynamic simulations, no data in the time scale of the simulation could be obtained (data not shown). Next, we constructed a model peptide that resembled the N-terminus where Ser17 resides (K9-E19 fragment). An initial estimate of the secondary structure was generated using the PSIPRED server and submitted to the AbinitioRelax application as implemented in Rosetta 3.0[13]. This application resulted in 5,000 possible structures and only conformations in structural agreement with the initial estimate were used in the second stage of this procedure. We chose the structure that permitted the accommodation of the phosphate group in the S17 position without disturbing the structure of the peptide (Supplementary Fig. S5a–b).

To identify possible cavities in the structure of the protein where the peptide could interact, we subjected the inactive structure of c-Src to a Computed Atlas of Surface Topography of Proteins (CASTp)[14] analysis using the University of California at San Francisco Chimera interface. The obtained results suggested three possible cavities with an area and volume large enough to accommodate the designed peptide (Figure 4b and Supplementary Fig. S5c). One of these cavities is the active site where ANP binds, which is not spatially accessible for the peptide until the protein is in its active conformation. To elucidate which of the cavities was the best candidate, the structure of Src was compared to the human tyrosine kinase c-Abl, (PDB code: 2fo0). Both of these structures were aligned using the Multiseq plug-in[15] in the Visual Molecular Dynamics package (VMD 1.8.4)[16]. c-Abl has a different auto inactivation mechanism compared with c-Src. However, this mechanism involves interaction of the N-terminal Myristoyl group with the 4 major helices (H11, H16, H18, and H20) in the kinase domain. This structure includes residues 65 to 82 that are part of the N- terminal cap of c-Abl. Due to the structural resemblance between Src and c-Abl (47% sequence homology)[17], it is plausible that the conformation of the N-terminus in c-Abl is similar to the N-terminus in Src, and hence it is possible to conclude that the N-terminus of c-Src follows a similar trajectory as the N-terminus of c-Abl, a trajectory that is well known. Based on this analysis, Src has only one possible cavity where the peptide can be inserted. This cavity is located near the C-terminal, and between the SH2 and kinase domain (Figure 4b and Supplementary Fig. S5c). This cavity is also the most accessible of the three cavities we identified. Furthermore, we used molecular dynamics to simulate a hydrated Src and performed solvation analyses[18–20] of the selected cavity to ensure that water displacement from the allosteric site is thermodynamically favorable. This approach identified eight high solvent density regions in the cavity that are thermodynamically unfavorable and displaced after the peptide binds. Water displacement from these regions to more thermodynamically favorable bulk biological fluid strongly suggests that the peptide can bind at this site (Supplementary Fig. S5d).

Since the peptide contains a high content of charged residues (63.6%), a charge distribution analysis was performed using the Adaptive Poisson-Boltzmann Solver (APBS) within

Pymol[21] while the charges and radii used were obtained from the amber99SB force field[22]. Our results demonstrated that the chosen cavity had a highly negative charged surface in the interior that could accommodate the positive portion of the peptide while exhibiting a positively charged entrance that could accommodate the negative charge on the other part of the peptide (Figure 4c–e). Hence, from an electrostatic point of view, this cavity provides the correct environment for protein-peptide interaction.

Finally, we performed molecular dynamic simulations using the inactive structure of c-Src with the phosphorylated peptide docked to the cavity that we identified in our previous simulations. Our results demonstrate that the Src/phosphorylated peptide model undergoes significant structural changes in the kinase domain, i.e. exposure of the Y419 residue without alteration of the C-terminus (Figure 4f, Supplementary Movie 1). Additionally, our simulation showed that the SH2 domain maintained its closed conformation. These two changes are characteristic of the activated form of Src. Supplementary Figure S5e depicts a probability contour of the contacts between the phosphorylated peptide and the protein throughout the simulated timeframe. In contrast, a peptide containing a S17A mutation had a negligible difference in its polarity when compared to an unphosphorylated peptide and due to size of this system, we assumed this difference to be insignificant. Hence, we performed simulations of Src in the presence of a peptide lacking S17 phosphorylation. Furthermore, no significant alteration of the protein structure was observed when the simulation was run with this peptide (Figure 4g and Supplementary Movie 2). Moreover, during the simulated time, the unphosphorylated peptide leaves the cavity, suggesting that the interaction between the peptide and Src is not as strong as with the phosphorylated peptide. To confirm these results, we performed a kinase assay where Src was exposed to the same phosphorylated peptide used in our molecular dynamic simulations. Upon interaction with the phosphorylated peptide, Src^{Y419} phosphorylation was substantially elevated, resulting in enhanced enzymatic activity and increased Src-dependent FAK phosphorylation at Y861 (Supplementary Fig. S5f–h).

Src mediates NE-induced cell migration and invasion

To determine the functional effects of NE-induced Src^{S17} phosphorylation, we first examined its effects on cell migration. In WT Src-transfected SYF cells, NE increased S17 phosphorylation, while PDGF treatment did not (Fig. 3d). Furthermore, NE and PDGF treatment significantly increased migration of WT Src–transfected SYF cells ($P < 0.01$). In contrast, NE did not stimulate the migration of S17A Src–transfected SYF cells, while PDGF still promoted cell migration ($P < 0.01$; Fig. 3d). In non-transfected SYF cells, NE failed to induce an increase in the migratory ability of these cells (Supplementary Fig. S4i). These data indicate that NE-induced Src activation requires direct phosphorylation of S17, which results in Src^{Y419} phosphorylation, a mechanism distinct from Src activation by classic growth factor/growth factor receptor interactions.

To determine whether Src or PKA were responsible for mediating the stimulatory effects of catecholamines, we used three different Src siRNA sequences that silenced Src expression by >80%, AP23846 or KT5720 (Supplementary Fig. S6a and data not shown). NE treatment significantly increased the invasive potential of SKOV3ip1 and HeyA8 cells ($P <0.01$; Fig.

5a and Supplementary Fig. S6c–d). Src siRNA or AP23846 completely abrogated the NE-induced increase in invasion in both cell lines (Fig. 5a and Supplementary Fig. S6c), while KT5720 blocked NE-induced invasion in SKOV3ip1 cells (Supplementary Fig. S6d). Furthermore, NE-induced migration of SKOV3ip1 or HeyA8 cells was abrogated with Src siRNA treatment or AP23846 (Fig. 5b and Supplementary Fig. S6b). Next, we used the poorly invasive A2780-ADRB2 cells because they express very low levels of Src when compared to a panel of ovarian cancer cells (data not shown). After transiently transfecting these cells with a vector carrying either WT Src or S17A Src, invasion assays were carried out. WT Src potentiated the effect of NE on the invasiveness of these cells, while the introduction of S17A Src failed to have a similar effect when compared to non-transfected A2780-ADRB2 cells (Supplementary Fig. S6e). Additionally, we transfected ID8^{VEGF} murine ovarian carcinoma cells with human WT Src or S17A Src and then silenced endogenous Src by treating them with siRNA targeted against murine Src. Cells were then exposed to NE and subjected to migration and invasion assays. NE treatment resulted in increased cancer cell migration and invasion in WT Src-ID8^{VEGF} cells, but not in the S17A Src-ID8^{VEGF} cells (Supplementary Fig. S6f–g).

We next asked if an increase in Src activity, upon adrenergic stimulation, could result in the induction of genes known to be mediators of cell motility and invasion. To address this question, we performed a cDNA microarray analysis of NE-treated SKOV3ip1 cells and identified genes relevant for tumor cell invasion. Our analysis revealed a significant increase in several such genes following NE treatment, and this increase was blocked by Src silencing (Supplementary Fig. S6h).

Restraint stress-induced tumor growth is mediated by Src

To test the biological significance of adrenergic-mediated Src activation, we utilized an *in vivo* restraint stress model[2]. In this model, tumors from animals exposed to daily restraint had substantially increased levels of pSrc^{Y419} (Supplementary Fig. S7b) compared to controls. Src siRNA was incorporated into 1,2-dioleoyl-sn-glycero-3-phosphatidylcholine (DOPC) nanoliposomes for *in vivo* delivery. After confirming >80% reduction in Src levels *in vivo* (Supplementary Fig. S7a), we treated control or restrained mice (n = 10 per group) bearing SKOV3ip1 or HeyA8 tumors with control siRNA-DOPC or Src siRNA-DOPC. As expected, daily restraint significantly increased tumor growth (Fig. 5c–d). This increase was completely blocked by Src siRNA-DOPC (Fig. 5c–d). Furthermore, the number of tumor nodules was also reduced by Src siRNA-DOPC in both the HeyA8 and SKOV3ip1 models (Fig. 5c–d). These results were confirmed by additional experiments that utilized two different Src-specific siRNA sequences and the Src small molecule inhibitor, AP23846 (Supplementary Fig. S7c–d). Next, we analyzed tumor tissues from daily restraint *versus* control mice that were treated with control siRNA or Src-specific siRNA with the proliferation markers phospho-histone h3 and proliferating cell nuclear antigen (PCNA) and the apoptotic marker cleaved caspase 3. Restraint stress resulted in increased cell proliferation that was abrogated by Src siRNA treatment (Supplementary Fig. S7e–f). There were no significant changes in apoptosis between any groups (data not shown). Since our data indicate that increased adrenergic signaling results in increased invasion *in vitro*, we analyzed H&E sections obtained from tumor bearing mice undergoing restraint stress. These

results show that restraint stress leads to tumor infiltration into underlying tissue and Src siRNA-DOPC abrogates this effect (Supplementary Fig. S7g). Moreover, we found that tumors from mice undergoing restraint stress had elevated β-catenin levels, while Src siRNA-DOPC blocks this increase (Supplementary Fig. S7h).

To determine the contribution of ADRB in the daily restraint model, we treated control or restrained mice (n = 10 per group) bearing HeyA8 tumors with propranolol. As expected, propranolol abrogated the daily restraint-induced increase in tumor growth (Fig. 5e). Tumors from animals treated with propranolol and exposed to daily restraint stress had substantially decreased levels of $pSrc^{Y419}$ compared with mice exposed to daily restraint stress (Supplementary Fig. S7i). To further delineate the role of ADRB on tumor growth, we treated HeyA8 tumor bearing mice (n = 10 mice) with either isoproterenol, xamoterol, terbutaline or isoproterenol plus propranolol. As expected, isoproterenol significantly increased tumor growth, and a similar increase in tumor burden was noted with terbutaline (Fig. 5f). However, treatment with xamoterol or propranolol in combination with isoproterenol did not result in increased tumor growth compared to the control group (Fig. 5f). Tumors from animals exposed to isoproterenol or terbutaline had substantially increased levels of $pSrc^{Y419}$ and $pSrc^{S17}$, while xamoterol or propranolol in combination with isoproterenol did not induce phosphorylation at these sites (Supplementary Fig. S7j). Additionally, bioluminescence imaging analysis revealed that daily restraint stress resulted in significantly increased tumor growth and metastasis, which was abrogated by the use of propranolol (Supplementary Fig. S7k). Next, to determine the effects of daily restraint stress on the patterns of metastasis, we utilized a fully orthotopic mouse. SKOV3ip1 ovarian cancer cells were injected directly into the right ovary of nude mice followed by exposure to daily restraint stress, with or without Src siRNA-DOPC treatment. Daily restraint stress resulted in significantly higher tumor nodule counts and distant metastatic spread compared with control siRNA-DOPC (Supplementary Fig. S7l). Src siRNA-DOPC completely abrogated the effects of stress on tumor metastasis (Supplementary Fig. S7l). To further delineate the role of ADRB2 *in vivo*, we inoculated mice (n = 7 per group) with A2780-OG2 (empty vector), A2780-ADRB2 or A2780 cells into the subcutaneous space and treated groups with isoproterenol or PBS. Isoproterenol significantly increased tumor growth in the A2780-ADRB2 group compared to the A2780-OG2 group while the A2780 group did not respond to isoproterenol treatment (Supplementary Fig. S7m). To examine the role of increased peripheral nervous system activity on tumor growth, we performed an experiment where mice undergoing daily restraint stress were inoculated with SKOV3ip1 cells and treated with the peripheral ganglionic blocker hexamethonium bromide (daily dose of 1 mg/kg). This treatment completely blocked the daily restraint-induced tumor growth (data not shown). Next, we used $ID8^{VEGF}$ murine ovarian cancer cells transfected with human WT Src or S17A mutated Src. These cells were then injected subcutaneously into the right flank of C57 mice, treated with murine Src siRNA-DOPC (to silence endogenous Src; Supplementary Fig. S7n) and isoproterenol. Isoproterenol treatment resulted in significantly increased tumor growth in mice inoculated with WT Src-cells, but not with S17A Src-cells (Supplementary Fig. S7n).

pSrc^{Y419} expression in human ovarian carcinoma

To determine whether adrenergic activity might relate to Src activation in human cancers, we examined 91 invasive epithelial ovarian cancers. Consistent with prior reports[23,24], increased Src expression was noted in 88% of the tumor samples, while elevated pSrc^{Y419} expression was noted in 42% (Fig. 6a). We found that elevated levels of pSrc^{Y419} were associated with poor mean patient survival by univariate analysis (1.67 years *versus* not yet reached; $P < 0.001$; Fig 6b). Since depression, as measured by high scores on the Center for Epidemiological Studies Depression scale (CESD) [25,26], has been linked to increased tumor catecholamine levels[27,28], we examined potential relationships between CESD scores and Src activity. Patients with high CESD scores (≥16) had significantly higher levels of tumoral pSrc^{Y419} ($P = 0.008$) compared to those with low scores (Fig. 6c). In addition, NE levels above the median were significantly associated with increased pSrc^{Y419} expression ($P < 0.001$), but not with increases in total Src (Fig. 6c). In a subset of these tumor samples, pSrc^{Y419} and pSrc^{S17} levels were evaluated by ELISA and Western blot analyses, respectively. There was a significant association between elevated pSrc^{Y419} and pSrc^{S17} in these samples (Supplementary Fig. S8a). Moreover, we found a strong positive correlation between tumoral NE and pSrc^{Y419} and pSrc^{S17} levels (Supplementary Fig. S8b–c).

Beta-blockers may reduce cancer-related mortality

To examine the potential clinical impact of our findings, we asked whether chemical perturbation of beta-adrenergic function in cancer patients might result in lower patient mortality. To test this hypothesis, we employed adverse events data from the FDA's Adverse Event Reporting System (AERS; http://www.fda.gov/Drugs/GuidanceComplianceRegulatoryInformation/Surveillance) to examine whether usage of beta-blockers by patients affected cancer related mortality. Our analysis revealed that mortality (i.e., "Death" reported either as a patient's outcome or as a patient' reaction), was reduced by an average of 17% across all major cancer types if patients were treated with beta-blockers (Fig. 6d). Moreover, a 14.64% decrease in mortality was observed among patients with ovarian and cervical cancer. These data suggest that beta blocker use among cancer patients can significantly reduce cancer related mortality.

DISCUSSION

Here, we describe a unique mechanism by which increased adrenergic signaling results in Src activation, which induces downstream proteins important for cell survival, motility, and invasion[29–31]. Increased serine phosphorylation at Src amino terminus following cAMP treatment was demonstrated 30 years ago[32], and a consensus PKA site at Src^{S17} was subsequently identified[33]. However, no physiological role for phosphorylation at Src^{S17} had been established; pSrc^{S17} can mediate Rap1 activation and inhibit ERK by cAMP-dependent pathways[34,35]. Src has been implicated in NE-stimulated VEGF production by adipocytes[36,37], and in NE-stimulated IL-6 production by cancer cells[7]. While different mechanisms have been suggested to account for ADRB-mediated Src activation (e.g., β-arrestin and EGFR-dependent Src phosphorylation[38]), the precise mechanisms mediating ADRB/cAMP/PKA-induced Src activation or the resultant biological effects were not well understood. Our results have identified a new functional role for Src^{S17} as a key molecular

switch that links a serine kinase to downstream tyrosine kinase signaling and disease progression (Fig. 6e). Specifically, our results indicate that the neuroendocrine stress response can directly affect tumor growth and malignant progression through receptors expressed on tumor cells that lead to a critical phosphorylation event, resulting in Src activation. Norepinephrine is the most abundant stress hormone in the ovary[39,40] and its levels are much higher in the ovary than in the plasma[41,42]. To the extent that biobehavioral states can modulate catecholamine levels in the tumor microenvironment, these findings offer new opportunities for designing interventions to protect individuals from the harmful effects of chronic adrenergic stimulation[43].

A number of studies have recently emerged supporting the rationale for designing clinical studies to target neuroendocrine function, which could represent a new avenue for treating individuals with cancer[44]. On the basis of our work, beta-antagonists can abrogate many of the deleterious effects of increased adrenergic signaling. For example, among prostate cancer patients taking anti-hypertensive medication, only beta blockers were associated with a reduction of cancer risk[44] while others have shown a reduction in overall cancer risk[45]. Moreover, our findings support the use of Src family kinase inhibitors as tools to block the deleterious effects of increased sympathetic activity[46,47]. Collectively, our data represent a new understanding of Src regulation in response to adrenergic signaling in cancer cells and provide a biologically plausible and potent way of inhibiting tumor progression among cancer patients.

METHODS

Proteomic Analysis

Two-dimensional gel electrophoresis was conducted as first described by O'Farrell[48]. All biological samples were run in duplicate (technical). After electrophoresis, the gels were fixed and either directly stained with SYPRO-Rube (Bio-Rad, Hercules, CA) or sequentially stained with ProQ-Diamond (detects phosphate groups attached to tyrosine, serine or threonine residues) and SYPRO-Ruby (detects total protein). Gels were then scanned at a 100-mm resolution using the Perkin-Elmer ProEXPRESS 2D Proteomic Imaging System (Boston, MA). After quantifying the relative spot intensities among samples and normalizing the phosphorylation levels to the total amount of protein, gel spots were excised and prepared for MALDI-TOF-MS analysis using DigiLab's (Holliston, MO) ProPic and ProPrep robotic instruments following the manufacturer's protocol. MALDI-TOF/TOF was performed using the Applied Biosystems 4800 MALDI TOF/TOF Analyzer for peptide mass fingerprinting and sequencing (See Supplementary Procedures for a more detailed description). Protein identification was performed using a Bayesian algorithm, where high probability matches are indicated by an expectation score, which is an estimate of the number of matches that would be expected in that database if the matches were completely random[49]. See Supplementary Procedures for expanded methodology.

Signaling Network Analysis

We sought to analyze whether a key mediator kinase might exist that is capable of directly or indirectly explaining the majority of the observed differences in phosphorylation and

protein abundance. We restricted the length of signaling chains to include at most two phosphorylation events (equivalently, allowing for at most one intermediate kinase, because otherwise, the set of potential candidates would suffer from "combinatorial explosion". We constructed this two-layer phosphorylation network upstream of the identified proteins using information from Phospho.ELM and networKIN [50,51]. In the resultant network, 45 of the dysregulated proteins could be linked to at least one of 243 kinases. Scoring and sorting these candidates by the number of downstream dysregulated proteins suggested Src as a tentative key mediator for the experimentally observed differences (37/45 proteins, Figure 1 and Supplementary Fig. S2a). We note that this neither disproves an important role for other kinases nor proves that Src is the most important kinase in this context; however it does illustrate some potential for Src being of central importance in the cellular response to NE.

Western Blot Analysis

Cell lysates were prepared by washing cells with phosphate-buffered saline and incubating them for 10 min at 4°C in modified radioimmunoprecipitation assay lysis buffer. Cells were scraped from plates and centrifuged for 20 min at 4oC, and the supernatant was collected. Protein concentrations were determined using a BCA reagent kit (Pierce), and 40 μg of whole cell lysates were separated by 10% SDS-PAGE. Samples were transferred to a nitrocellulose membrane by wet electrophoresis (Bio-Rad), blocked with 5% nonfat milk for 1 h at room temperature, and incubated with Src, Src^{Y416}, or Src^{Y530} overnight at 4°C. Primary antibody was detected with anti-rabbit IgG (Amersham Biosciences, Piscataway, NJ) and developed with an enhanced chemiluminescence detection kit (Pierce, Rockford, IL).

siRNA Preparation and Treatment

We used small interfering RNA (siRNA) to downregulate Src *in vitro* and *in vivo*. Src-specific siRNA was purchased from Ambion (Austin, TX) with the following target sequence: 5′-GGCTGAGGAGTGGTATTTT-3′. Additional validated Src sequences were purchased from Sigma-Genosys (The Woodlands, TX). Control siRNA used was obtained from Qiagen (Valencia, CA) with the following target sequence: 5′-AATTCTCCGAACGTGTCACGT-3′. For *in vitro* studies, cells were transfected with siRNA that was incorporated into Lipofectamine 2000 transfection reagent (Invitrogen, Carlsbad, CA) following the manufacturer's protocol. After 72 h, the experiments were carried out. For *in vivo* studies, siRNA was incorporated into the neutral liposome 1,2-dioleoyl-sn-glycero-3-phosphatidylcholine (DOPC) as previously described[52,53]. For each treatment, 3.5 μg of siRNA was reconstituted in 200 μL of phosphate buffered saline and administered by intravenous injection. The dosing schedule is described in the *in vivo* tumor model below.

Migration and Invasion Assay

The membrane invasion culture system (MICS) chamber was used to measure the *in vitro* invasive and migratory potential of all cell lines used in this study. When required, siRNA was added to cells 24 h prior to cell harvest, and NE was added at the start of the experiment. The MICS assay was performed as previously described. Briefly, single cell

tumor suspensions were seeded into the upper wells at a concentration of 1 X 10^5 cells per well for the invasion assays and 7.5 X 10^4 cells per well for the migration assays. For the invasion and migration assays, a human basement membrane and gelatin-coated membrane were used, respectively. Cells were allowed to invade for 24 h or migrate for 6 h for the invasion and migration assays, respectively. The cells were then collected, fixed, stained, and counted by light microscopy.

Chronic Stress Model

We obtained 8- to 12-week-old female athymic nude mice from the National Cancer Institute. All experiments were approved by the Institutional Animal Care and Use Committee at M. D. Anderson Cancer Center. To experimentally induce stress in the mice, we used a restraint-stress procedure that utilizes a physical restraint system that we developed. Tumor cells were injected intraperitoneally or subcutaneously into mice in all groups 7 days after the stress procedure began. A total of 10 mice per group were used. Starting 4 days after tumor cell injection, mice were treated with siRNA (control or Src-specific, 3.5 μg in DOPC every 3 days, intraperitoneally) for the duration of the experiments. We necropsied the animals 21 days after tumor cell injection. At this time, the entire peritoneal cavity was examined for identifiable disease, and mouse weight, tumor weight, and the distribution of tumor was recorded by gynecologic oncologists.

Center for Epidemiological Studies Depression Scale (CES-D)

Patients completed psychosocial questionnaires between their initial preoperative appointment and surgery. The CES-D scale is a 20-item measure that assesses depressive symptomatology over the last week [25]. Scores of 16 or higher have been associated with clinical depression.

Statistical Analysis

We compared continuous variables using either Student's t-test or analysis of variance and compared the categorical variables using the chi-squared test. We used a nonparametric test (Mann-Whitney test), when appropriate, to compare differences. We considered $P < 0.05$ to be significant.

Additional Methods

Details of reagents, cell culture conditions, mass spectrometry, protein identification analysis, microarray analysis, plasmids, kinase assay, immunochemistry, immunoprecipitation and methods used to determine norepinephrine concentration, molecular dynamic simulations and the bioinformatics analysis of the FDA adverse event reports can be found in the Supplementary Methods.

Supplementary Material

Refer to Web version on PubMed Central for supplementary material.

Acknowledgments

GNA-P was supported, in part, by the NCI F31CA126474 Fellowship for Minority Students. YGL, LYH, AMN, and RLS were supported by an NIH T32 Training Grant CA101642. SKL was supported by NIH grants CA140933 and CA104825. MMS was supported by the GCF-Molly Cade ovarian cancer research grant and the NIH/NICHD Baylor WRHR scholarship grant. This work was also supported in part by NIH grants (CA110793 and CA109298, P50CA083639, P50CA098258, CA128797, RC2GM092599, U54CA151668, U54CA96300 and U54CA96297), the University of Texas Medical Branch NHLBI Proteomics Center (contract HV-10-05_(2)), Ovarian Cancer Research Fund Program Project Development Grant, Department of Defense (OC073399, W81XWH-10-1-0158, OC100237, and BC085265), the Zarrow Foundation, the Betty Ann Asche Murray Distinguished Professorship, the Marcus Foundation, the RGK Foundation, the Gilder Foundation, the estate of C. G. Johnson, Jr., the Laura & John Arnold Foundation) and the Blanton-Davis Ovarian Cancer Research Program. The authors thank Ms. Donna Reynolds and Drs. Robert Langley, and Philip Stork for helpful discussions, comments and for providing reagents. We would like to thank the High Performance Computing Facility of the University of Puerto Rico for the computer time.

References

1. Antoni MH, et al. The influence of bio-behavioural factors on tumour biology: pathways and mechanisms. Nature reviews Cancer. 2006; 6:240–248. [PubMed: 16498446]
2. Thaker PH, et al. Chronic stress promotes tumor growth and angiogenesis in a mouse model of ovarian carcinoma. Nature medicine. 2006; 12:939–944.
3. Sood AK, et al. Adrenergic modulation of focal adhesion kinase protects human ovarian cancer cells from anoikis. The Journal of clinical investigation. 2010; 120:1515–1523. [PubMed: 20389021]
4. Sood AK, et al. Stress hormone-mediated invasion of ovarian cancer cells. Clinical cancer research : an official journal of the American Association for Cancer Research. 2006; 12:369–375. [PubMed: 16428474]
5. Shahzad MM, et al. Stress effects on FosB- and interleukin-8 (IL8)-driven ovarian cancer growth and metastasis. The Journal of biological chemistry. 2010; 285:35462–35470. [PubMed: 20826776]
6. Landen CN Jr, et al. Neuroendocrine modulation of signal transducer and activator of transcription-3 in ovarian cancer. Cancer research. 2007; 67:10389–10396. [PubMed: 17974982]
7. Nilsson MB, et al. Stress hormones regulate interleukin-6 expression by human ovarian carcinoma cells through a Src-dependent mechanism. The Journal of biological chemistry. 2007; 282:29919–29926. [PubMed: 17716980]
8. Peleg D, Arbogast LA, Peleg E, Ben-Jonathan N. Predominance of L-dopa in fetal plasma and the amniotic fluid during late gestation in the rat. American journal of obstetrics and gynecology. 1984; 149:880–883. [PubMed: 6465252]
9. Lutgendorf SK, et al. Stress-related mediators stimulate vascular endothelial growth factor secretion by two ovarian cancer cell lines. Clinical cancer research : an official journal of the American Association for Cancer Research. 2003; 9:4514–4521. [PubMed: 14555525]
10. Thomas SM, Brugge JS. Cellular functions regulated by Src family kinases. Annual review of cell and developmental biology. 1997; 13:513–609.
11. Xu W, Harrison SC, Eck MJ. Three-dimensional structure of the tyrosine kinase c-Src. Nature. 1997; 385:595–602. [PubMed: 9024657]
12. Xu W, Doshi A, Lei M, Eck MJ, Harrison SC. Crystal structures of c-Src reveal features of its autoinhibitory mechanism. Molecular cell. 1999; 3:629–638. [PubMed: 10360179]
13. Trott O, Olson AJ. AutoDock Vina: improving the speed and accuracy of docking with a new scoring function, efficient optimization, and multithreading. Journal of computational chemistry. 2010; 31:455–461. [PubMed: 19499576]
14. Dundas J, et al. CASTp: computed atlas of surface topography of proteins with structural and topographical mapping of functionally annotated residues. Nucleic acids research. 2006; 34:W116–118. [PubMed: 16844972]
15. Roberts E, Eargle J, Wright D, Luthey-Schulten Z. MultiSeq: unifying sequence and structure data for evolutionary analysis. BMC bioinformatics. 2006; 7:382. [PubMed: 16914055]
16. Humphrey W, Dalke A, Schulten K. VMD: visual molecular dynamics. Journal of molecular graphics. 1996; 14:33–38. 27–38. [PubMed: 8744570]

17. Nagar B, et al. Structural basis for the autoinhibition of c-Abl tyrosine kinase. Cell. 2003; 112:859–871. [PubMed: 12654251]
18. Young T, Abel R, Kim B, Berne BJ, Friesner RA. Motifs for molecular recognition exploiting hydrophobic enclosure in protein-ligand binding. Proceedings of the National Academy of Sciences of the United States of America. 2007; 104:808–813. [PubMed: 17204562]
19. Lazaridis T. Inhomogeneous fluid approach to solvation thermodynamics. J phys chem b. 2011; 102:3531–3541.
20. Li Z, Lazaridis T. Computing the thermodynamic contributions of interfacial water. Methods Mol Biol. 2012; 819:393–404. [PubMed: 22183549]
21. Baker NA, Sept D, Joseph S, Holst MJ, McCammon JA. Electrostatics of nanosystems: application to microtubules and the ribosome. Proceedings of the National Academy of Sciences of the United States of America. 2001; 98:10037–10041. [PubMed: 11517324]
22. Simons KT, Bonneau R, Ruczinski I, Baker D. Ab initio protein structure prediction of CASP III targets using ROSETTA. Proteins Suppl. 1999; 3:171–176.
23. Wiener JR, et al. Activated SRC protein tyrosine kinase is overexpressed in late-stage human ovarian cancers. Gynecologic oncology. 2003; 88:73–79. [PubMed: 12504632]
24. Budde RJ, Ke S, Levin VA. Activity of pp60c-src in 60 different cell lines derived from human tumors. Cancer biochemistry biophysics. 1994; 14:171–175. [PubMed: 7537173]
25. Radloff LS. The CES-D scale. Social support, life events, and depression. Appl Psychol Meas. 1977; 1:385–401.
26. Ensel, WM. Social support, life events, and depression. Academic Press; 1986. Measuring depression: the CES-D scale.
27. Lutgendorf SK, et al. Depression, social support, and beta-adrenergic transcription control in human ovarian cancer. Brain, behavior, and immunity. 2009; 23:176–183.
28. Hughes JW, Watkins L, Blumenthal JA, Kuhn C, Sherwood A. Depression and anxiety symptoms are related to increased 24-hour urinary norepinephrine excretion among healthy middle-aged women. Journal of psychosomatic research. 2004; 57:353–358. [PubMed: 15518669]
29. Kim MJ, et al. Downregulation of FUSE-binding protein and c-myc by tRNA synthetase cofactor p38 is required for lung cell differentiation. Nature genetics. 2003; 34:330–336. [PubMed: 12819782]
30. Obermeier A, et al. PAK promotes morphological changes by acting upstream of Rac. The EMBO journal. 1998; 17:4328–4339. [PubMed: 9687501]
31. Meylan E, Martinon F, Thome M, Gschwendt M, Tschopp J. RIP4 (DIK/PKK), a novel member of the RIP kinase family, activates NF-kappa B and is processed during apoptosis. EMBO reports. 2002; 3:1201–1208. [PubMed: 12446564]
32. Cross FR, Hanafusa H. Local mutagenesis of Rous sarcoma virus: the major sites of tyrosine and serine phosphorylation of pp60src are dispensable for transformation. Cell. 1983; 34:597–607. [PubMed: 6311433]
33. Brown MT, Cooper JA. Regulation, substrates and functions of src. Biochimica et biophysica acta. 1996; 1287:121–149. [PubMed: 8672527]
34. Obara Y, Labudda K, Dillon TJ, Stork PJ. PKA phosphorylation of Src mediates Rap1 activation in NGF and cAMP signaling in PC12 cells. Journal of cell science. 2004; 117:6085–6094. [PubMed: 15546918]
35. Schmitt JM, Stork PJ. PKA phosphorylation of Src mediates cAMP's inhibition of cell growth via Rap1. Molecular cell. 2002; 9:85–94. [PubMed: 11804588]
36. Fredriksson JM, Nedergaard J. Norepinephrine specifically stimulates ribonucleotide reductase subunit R2 gene expression in proliferating brown adipocytes: mediation via a cAMP/PKA pathway involving Src and Erk1/2 kinases. Experimental cell research. 2002; 274:207–215. [PubMed: 11900481]
37. Fredriksson JM, Lindquist JM, Bronnikov GE, Nedergaard J. Norepinephrine induces vascular endothelial growth factor gene expression in brown adipocytes through a beta -adrenoreceptor/cAMP/protein kinase A pathway involving Src but independently of Erk1/2. The Journal of biological chemistry. 2000; 275:13802–13811. [PubMed: 10788502]

38. Gschwind A, Zwick E, Prenzel N, Leserer M, Ullrich A. Cell communication networks: epidermal growth factor receptor transactivation as the paradigm for interreceptor signal transmission. Oncogene. 2001; 20:1594–1600. [PubMed: 11313906]
39. Aguado LI, Ojeda SR. Prepubertal ovarian function is finely regulated by direct adrenergic influences. Role of noradrenergic innervation. Endocrinology. 1984; 114:1845–1853. [PubMed: 6325133]
40. Ben-Jonathan N, Arbogast LA, Rhoades TA, Bahr JM. Norepinephrine in the rat ovary: ontogeny and de novo synthesis. Endocrinology. 1984; 115:1426–1431. [PubMed: 6434292]
41. Lara HE, et al. Changes in sympathetic nerve activity of the mammalian ovary during a normal estrous cycle and in polycystic ovary syndrome: Studies on norepinephrine release. Microscopy research and technique. 2002; 59:495–502. [PubMed: 12467025]
42. Schmidt C, Kraft K. Beta-endorphin and catecholamine concentrations during chronic and acute stress in intensive care patients. European journal of medical research. 1996; 1:528–532. [PubMed: 9438155]
43. Armaiz-Pena GN, Cole SW, Lutgendorf SK, Sood AK. Neuroendocrine influences on cancer progression. Brain, behavior, and immunity. 2012
44. Perron L, Bairati I, Harel F, Meyer F. Antihypertensive drug use and the risk of prostate cancer (Canada). Cancer causes & control : CCC. 2004; 15:535–541. [PubMed: 15280632]
45. Algazi M, Plu-Bureau G, Flahault A, Dondon MG, Le MG. Could treatments with beta-blockers be associated with a reduction in cancer risk? Revue d'epidemiologie et de sante publique. 2004; 52:53–65.
46. Kopetz S, Shah AN, Gallick GE. Src continues aging: current and future clinical directions. Clinical cancer research : an official journal of the American Association for Cancer Research. 2007; 13:7232–7236. [PubMed: 18094400]
47. Nam S, et al. Action of the Src family kinase inhibitor, dasatinib (BMS-354825), on human prostate cancer cells. Cancer research. 2005; 65:9185–9189. [PubMed: 16230377]
48. O'Farrell PH. High resolution two-dimensional electrophoresis of proteins. The Journal of biological chemistry. 1975; 250:4007–4021. [PubMed: 236308]
49. Ryckaert JPCG, Berendsen HJ. Numerical integration of the cartesian equations of motion of a system with constrains: Molecular Dynamics of n-alkenes. J Comput Phys. 1977; 23:327–341.
50. Diella F, et al. Phospho. ELM: a database of experimentally verified phosphorylation sites in eukaryotic proteins. BMC bioinformatics. 2004; 5:79. [PubMed: 15212693]
51. Linding R, et al. Systematic discovery of in vivo phosphorylation networks. Cell. 2007; 129:1415–1426. [PubMed: 17570479]
52. Landen CN Jr, et al. Therapeutic EphA2 gene targeting in vivo using neutral liposomal small interfering RNA delivery. Cancer research. 2005; 65:6910–6918. [PubMed: 16061675]
53. Pecot CV, Calin GA, Coleman RL, Lopez-Berestein G, Sood AK. RNA interference in the clinic: challenges and future directions. Nature reviews Cancer. 2011; 11:59–67. [PubMed: 21160526]

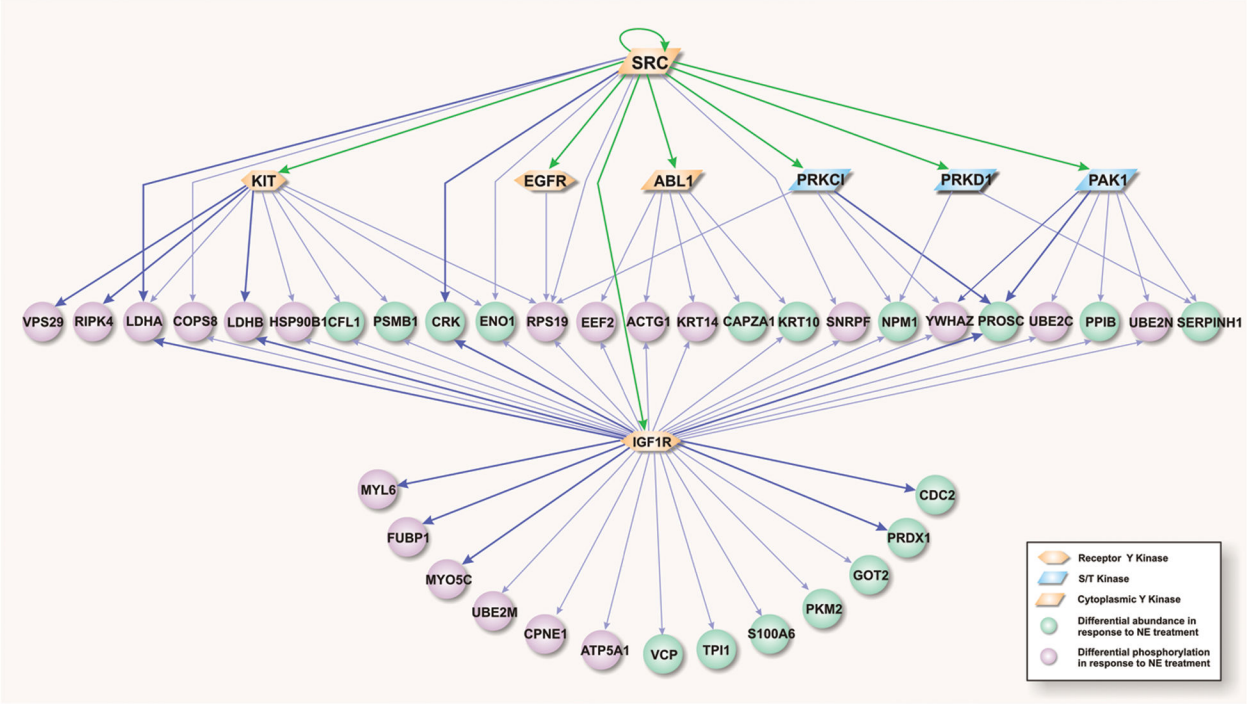

Figure 1. Putative phosphorylation cascade triggered by the NE-induced activation of Src

In this predicted network (see “Bioinformatics Analysis” in “Methods”), the components connecting Src to the NE-responsive proteins are shown as arrows: green, experimentally observed phosphorylation according to PhosphoELM; dark blue, predicted by NetworKIN; light blue, predicted by NetworKIN for a close homolog of the target.

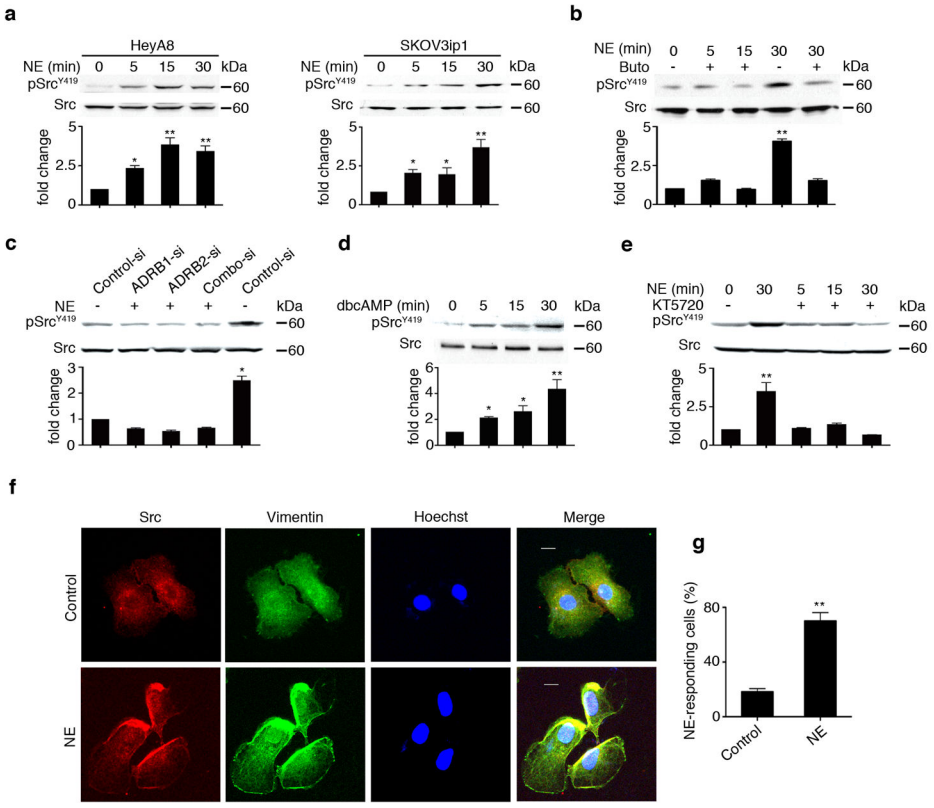

Figure 2. NE-induced Src activation is mediated by an ADRB/cAMP/PKA mechanism

(**a**) Effect of 10 μM NE on Src^{Y419} phosphorylation in HeyA8 and SKOV3ip1 cells. **P* < 0.01, ***P* < 0.001; two-tail Student's *t*-test (**b**) HeyA8 cells were incubated for 1h with 1 μM butoxamine (Buto, β_2 antagonist), exposed to 10 μM NE and probed for $pSrc^{Y419}$. **P* < 0.001; two-tail Student's *t*-test (**c**) Similar experiments were performed with siRNA targeted against ADRB1 (ADRB1 si) or ADRB2 (ADRB2 si) in SKOV3ip1 cells. **P* < 0.001; two-tail Student's *t*-test (**d**) Effect of 50 μM dbcAMP (PKA agonist) on $pSrc^{Y419}$ in SKOV3ip1 cells. **P* < 0.01, ***P* <0.001; two-tail Student's *t*-test (**e**) HeyA8 cells were exposed to 10 μM KT5720 (PKA antagonist) for 1 hr, stimulated with 10 μM NE, and probed for $pSrc^{Y419}$. **P* < 0.001; two-tail Student's *t*-test (**f**) SKOV3ip1 cells were treated with 10 μM NE, and Src was visualized by immunofluorescence (scale bar = 9.375 μm). **(g)** Quantification of cellular response to NE (measured as cells with increased Src expression at the focal adhesions) is shown in graphs **P* < 001; two-tail Student's *t*-test. In panels (**a–e,**), the immunoblot is shown at the top and quantification of pSrc band intensity relative to the intensity of the total Src band is shown below.

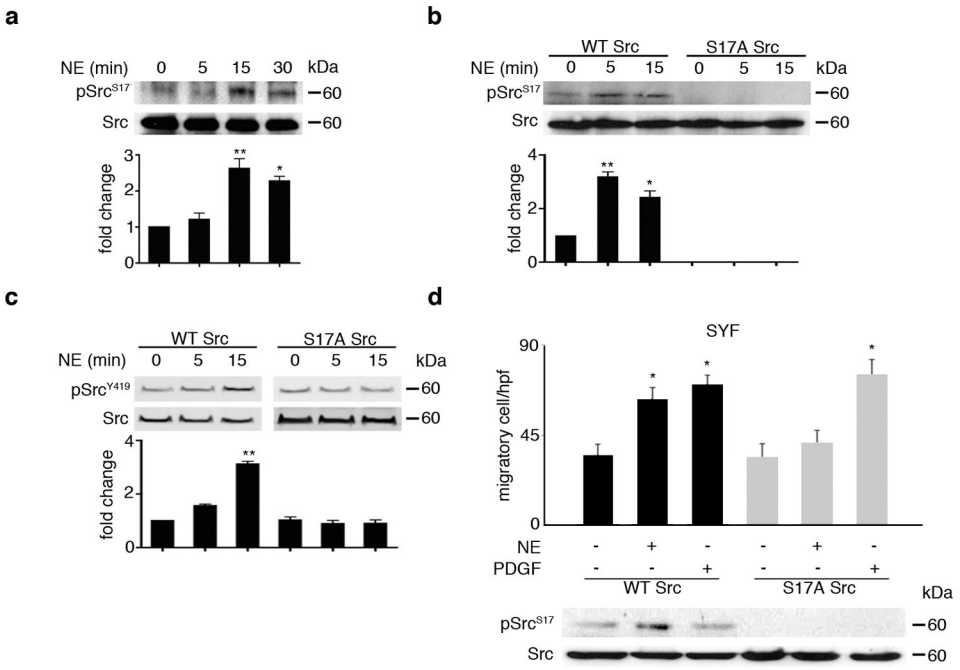

Figure 3. NE-induced Src^{S17} phosphorylation on SYF cells is required for Src activation

(**a**) HeyA8 cells were treated with 10 μM NE and probed for pSrc^{S17}. *P < 0.01; **P < 0.001; two-tail Student's t-test. SYF-null cells transfected with either WT or mutant Src (S17A) were stimulated with 10 μM NE and immunoblotted for (**b**) pSrc^{S17} or (**c**) pSrc^{Y419}. *P < 0.01; **P < 0.001; two-tail Student's t-test. (**d**) SYF-null cells transfected with either WT or mutant Src (S17A) were stimulated with 10 μM NE or PDGF (20 ng/mL) and subjected to a migration assay or Western blot analysis for pSrc^{S17} expression. *P < 0.01; two-tail Student's t-test. In panels (**a–c**), the immunoblot is shown at the top and quantification of pSrc band intensity relative to the intensity of the total Src band is shown below.

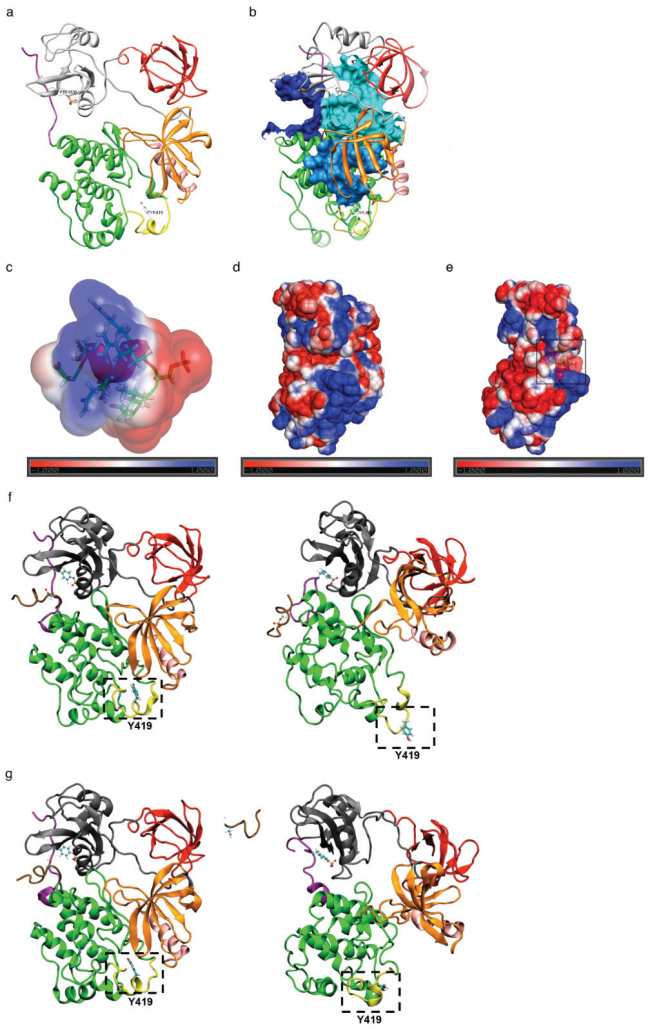

Figure 4. Interaction between pS17 and Src results in conformational changes that expose Y419

(a) Inactive form of the protein obtained from the protein data bank (PDB code: 2SRC). The phosphoaminophosphonic acid-adenylate ester (ANP) and all the water molecules were deleted from the PDB structure. **(b)** View of the three identified cavities where the peptide could be inserted. Charge distribution analysis of **(c)** designed model peptide, **(d)** Src, and **(e)** the model peptide docked in the proposed cavity. The red and blue regions represent negative and positive charges, respectively. **(f)** After the phospho-peptide was exposed to Src for 36 ns, the kinase domain moved, completely exposing Y419. **(g)** When Src was exposed to an unphosphorylated peptide, no significant movement was observed and Y419 was not exposed. The SH3, SH2, N-lobe, and alphaC domains are shown in red, gray, orange, and pink, respectively. The C-lobe, A-loop, C-terminus, and phosphopeptide are shown in green, yellow, purple, and brown, respectively.

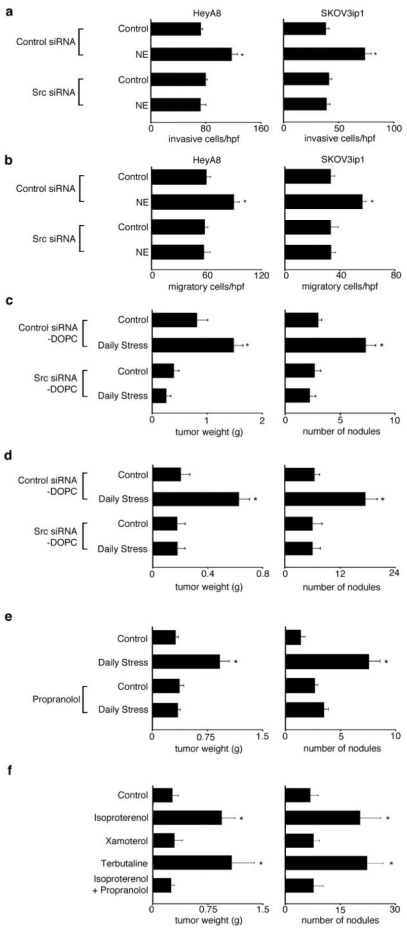

Figure 5. Adrenergic-mediated Src activation leads to increased tumor invasion and growth

NE 10 μM induces HeyA8 and SKOV3ip1 **(a)** cell invasion and **(b)** migration. **(c)** Mice were inoculated with either HeyA8 ($2.5x10^5$) or **(d)** SKOV3ip1 ($1.0x10^6$) cells and subjected to daily restraint and treated twice a week with either control siRNA-DOPC or Src siRNA-DOPC. Treatment with Src siRNA-DOPC blocked the daily restraint mediated induction in tumor weight and number of nodules compared to control siRNA-DOPC. (**e**) Mice bearing SKOV3ip1 tumors undergoing daily restraint were treated daily with propranolol (2 mg/kg). Propranolol counteracts the effects of daily restraint on tumor growth. **(f)** Mice bearing SKOV3ip1 tumors were treated daily with either: 10 mg/kg isoproterenol, 5 mg/kg terbutaline, 1 mg/kg xamoterol, or isoproterenol plus 2 mg/kg of propranolol. Isoproterenol and terbutaline induced tumor growth, but not xamoterol. Mice treated with isoproterenol plus propranolol have tumor burden similar to control mice.

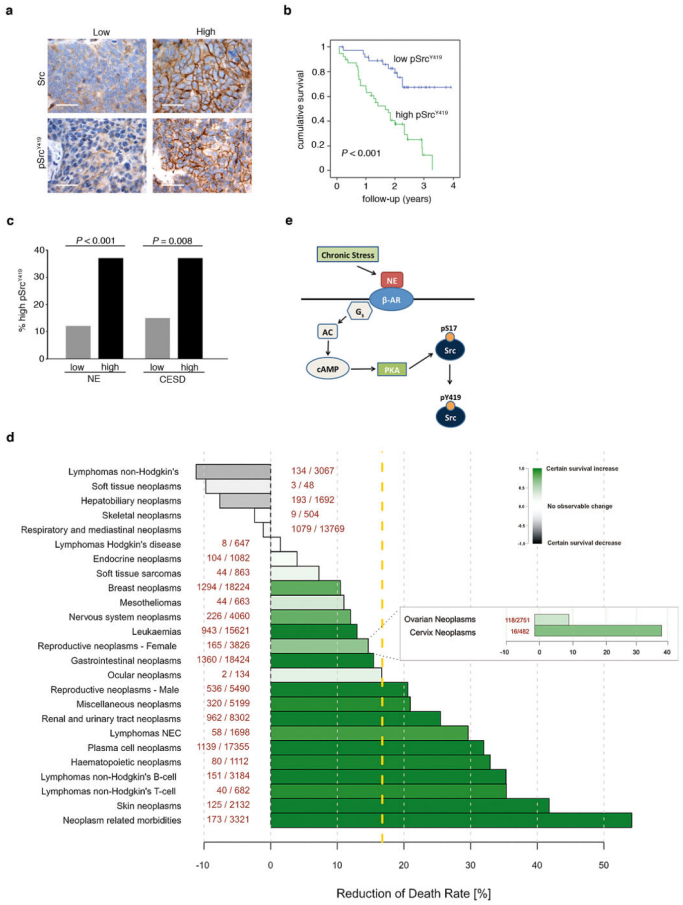

Figure 6. High pSrc^{Y419} levels are associated with decreased survival and depressive symptoms

(a) Representative images of human ovarian tumors with low or high expression of Src and pSrc^{Y419}. Images were taken at original magnification X200 (scale bar = 50 μm). **(b)** Kaplan-Meier curves of disease-specific mortality for patients with epithelial ovarian carcinoma (n= 91) based on pSrc^{Y419} expression. The log-rank test (two-sided) was used to compare differences between groups. **(c)** Percentage of ovarian cancers with high pSrc^{Y419} expression based on tumoral NE levels (greater than the median value of 0.84 pg/mg *versus* less than 0.84 pg/mg) and CESD scores ≥ 16. **(d)** Effect of beta blocker usage on cancer-related mortality, as estimated based on data from the FDA Adverse Event Reporting System. Bars, mortality decrease (green) or increase (black) by cancer type; saturation representing statistical confidence. Dashed yellow line, general mortality reduction over all cancer-related cases (17%). Numbers, cases having received a beta-blocker / total number of cases with given cancer type. **(e)** In response to chronic stress, catecholamines are released from the sympathetic nervous system. Stress-related hormones bind and activate ADRB receptors on tumor cells, initiating a cascade of events that result in Src activation.